The Journal of Immunology

G Protein–Coupled Receptor Kinase 6 Deficiency Promotes Angiogenesis, Tumor Progression, and Metastasis

Sandeep K. Raghuwanshi, Nikia Smith, Elizabeth J. Rivers, Ariel J. Thomas, Natalie Sutton, Yuhui Hu, Somnath Mukhopadhyay, Xiaoxin L. Chen, TinChung Leung and Ricardo M. Richardson

J Immunol 2013; 190:5329-5336; Prepublished online 15 April 2013;
doi: 10.4049/jimmunol.1202058
http://www.jimmunol.org/content/190/10/5329

The Journal of Immunology is published twice each month by
The American Association of Immunologists, Inc.,
1451 Rockville Pike, Suite 650, Rockville, MD 20852

Print ISSN: 0022-1767 Online ISSN: 1550-6606.

G Protein–Coupled Receptor Kinase 6 Deficiency Promotes Angiogenesis, Tumor Progression, and Metastasis

Sandeep K. Raghuwanshi,* Nikia Smith,* Elizabeth J. Rivers,* Ariel J. Thomas,* Natalie Sutton,* Yuhui Hu,* Somnath Mukhopadhyay,*,† Xiaoxin L. Chen,* TinChung Leung,*,‡ and Ricardo M. Richardson*

G protein–coupled receptor kinases (GRKs) phosphorylate the activated form of G protein–coupled receptors leading to receptor desensitization and downregulation. We have recently shown that the chemokine receptor, CXCR2, couples to GRK6 to regulate cellular responses including chemotaxis, angiogenesis, and wound healing. In this study, we investigate the role of GRK6 in tumorigenesis using murine models of human lung cancer. Mice deficient in GRK6 (GRK6$^{-/-}$) exhibited a significant increase in Lewis lung cancer growth and metastasis relative to control littermates (GRK6$^{+/+}$). GRK6 deletion had no effect on the expression of proangiogenic chemokine or vascular endothelial growth factor, but upregulated matrix metalloproteinase (MMP)-2 and MMP-9 release, tumor-infiltrating PMNs, and microvessel density. Because β-arrestin-2–deficient (βarr2$^{-/-}$) mice exhibited increased Lewis lung cancer growth and metastasis similar to that of GRK6$^{-/-}$, we developed a double GRK6$^{-/-}$/βarr2$^{-/-}$ mouse model. Surprisingly, GRK6$^{-/-}$/βarr2$^{-/-}$ mice exhibited faster tumor growth relative to GRK6$^{-/-}$ or βarr2$^{-/-}$ mice. Treatment of the mice with anti-CXCR2 Ab inhibited tumor growth in both GRK6$^{-/-}$ and GRK6$^{-/-}$/βarr2$^{-/-}$ animals. Altogether, the results indicate that CXCR2 couples to GRK6 to regulate angiogenesis, tumor progression, and metastasis. Deletion of GRK6 increases the activity of the host CXCR2, resulting in greater PMN infiltration and MMP release in the tumor microenvironment, thereby promoting angiogenesis and metastasis. Because GRK6$^{-/-}$/βarr2$^{-/-}$ showed greater tumor growth relative to GRK6$^{-/-}$ or βarr2$^{-/-}$ mice, the data further suggest that CXCR2 couples to different mechanisms to mediate tumor progression and metastasis. ***The Journal of Immunology*****, 2013, 190: 5329–5336.**

The G protein–coupled receptor kinases (GRKs) are a versatile family of kinases that play a critical role in G protein–coupled receptor homologous desensitization. GRKs phosphorylate specific serine and threonine residues in the cytoplasmic domains of the activated receptor, thereby promoting receptor–arrestin interaction and uncoupling of the receptor from its G protein (1). The GRK family consists of seven members (GRK1–7) with differing patterns of expression. GRK1 and GRK7 are restricted to the visual system; GRK4 is found predominantly in the testis, whereas GRK2, GRK3, GRK5, and GRK6 are expressed in all mammalian cells (1, 2). Although all GRKs have similar structural organization, they differ in their mechanisms of activation (2, 3). GRK2 and GRK3 are pleckstrin homology domain–containing proteins, which on receptor activation are recruited to the membrane by Gβγ (4–6). GRK4, GRK5, and GRK6, however, are membrane-associated proteins and are directly activated by the receptor–ligand complex (7–9).

CXCR2 is a member of the CXC subfamily of chemokine receptors that interacts with CXCL1, CXCL2, CXCL3, CXCL5, CXCL7, and CXCL8 with high affinity (10, 11). A hallmark of this subset of chemokines is the expression of a glutamic acid-leucine-arginine (ELR) motif in their N terminus, which appears to be critical for receptor-mediated angiogenesis (12, 13). Upon activation by ligand, CXCR2 becomes desensitized and downregulated (14–16). Desensitization of CXCR2 occurs via two mechanisms: protein kinase C dependent or heterologous, and GRK-dependent or homologous (14, 17, 18). We have recently shown that CXCR2 homologous desensitization occurs predominantly through phosphorylation of the receptor by GRK6 (19). Murine neutrophils and RBL-2H3 cells deficient in GRK6 expression exhibited diminished CXCR2 phosphorylation, desensitization, and downregulation (19). GRK6$^{-/-}$ mice also displayed greater neutrophil accumulation at the site of inflammation, enhanced angiogenesis, and faster wound closure relative to wild type (WT; GRK6$^{+/+}$) animals, indicating augmentation of CXCR2-dependent functions (19). These results mirrored those previously obtained with the β-arrestin-2–deficient (βarr2$^{-/-}$) mouse model and suggest that CXCR2 downmodulation via the GRK6/βarr2 axis is critical in modulating inflammatory responses (20, 21).

We have previously demonstrated that βarr2$^{-/-}$ mice displayed faster tumor growth and metastasis relative to WT animals (21). This effect was shown to be mediated via increased CXCR2-mediated NF-κB activation (21). Because GRK-mediated phosphorylation is critical for βarr2 association with the receptor, we

*Department of Biology, Julius L. Chambers Biomedical/Biotechnology Research Institute, North Carolina Central University, Durham, NC 27707; †Department of Chemistry, Julius L. Chambers Biomedical/Biotechnology Research Institute, North Carolina Central University, Durham, NC 27707; and ‡Nutrition Research Institute, North Carolina Research Campus, Kannapolis, NC 28081

Received for publication July 25, 2012. Accepted for publication March 4, 2013.

This work was supported by National Institutes of Health Grants AI38910, CA156735, NIMHD P20 MD00175, and U.S. Army Medical Research and Materiel Command Grant 07-1-0418 (all to R.M.R.) and by North Carolina Biotechnology Center Grant 2009-BRG-1213 (to T.L.).

Address correspondence and reprint requests to Dr. Ricardo M. Richardson, Julius L. Chambers Biomedical/Biotechnology Research Institute, North Carolina Central University, 1801 Fayetteville Street, Durham, NC 27707. E-mail address: mrrichardson@nccu.edu

The online version of this article contains supplemental material.

Abbreviations used in this article: βarr2, β-arrestin-2; ELR, glutamic acid-leucine-arginine; GRK, G protein–coupled receptor kinase; KC or CXCL1, keratinocyte-derived chemokine; LLC, Lewis lung cancer; MMP, matrix metalloproteinase; VEGF, vascular endothelial growth factor; WT, wild type.

www.jimmunol.org/cgi/doi/10.4049/jimmunol.1202058

hypothesized that GRK6 inhibition could also promote CXCR2-mediated tumor progression and metastasis. To test this hypothesis, we have used murine models of heterotopic Lewis lung cancer (LLC) and tail vein lung metastasis in GRK6$^{-/-}$ mice, GRK6$^{-/-}$/βarr2$^{-/-}$ double-knockout, and control littermates. The data in this study indicated that GRK6 depletion promoted angiogenesis, tumor development, and lung metastasis. These effects appear to be mediated through increased activation of the receptor leading to greater PMN accumulation and protease release in the tumor microenvironment, thereby promoting angiogenesis and tumor metastasis. Interestingly, GRK6$^{-/-}$/βarr2$^{-/-}$ animals showed greater tumor growth than that of GRK6$^{-/-}$ or βarr2$^{-/-}$. Taken together, the data indicate that CXCR2 couples to different mechanisms to promote angiogenesis and tumor development.

Materials and Methods

Materials

Lewis Lung carcinoma cell line (CRL-1642) was purchased from American Type Culture Collection. Anti-CD3, CD4, CD8a, CD45, NK1.1, and Ly6 were purchased from BD Pharmingen. Anti-CXCR2, keratinocyte-derived chemokine (CXCL1/KC), CXCL2/MIP-2, vascular endothelial growth factor (VEGF), matrix metalloproteinase-2 (MMP-2), and MMP-9 Abs; recombinant murine CXCL1/KC, CXCL2/MIP-2, CXCL12/SDF1, VEGF, MMP-2, and MMP-9 proteins; MMP-2 and MMP-9 ELISA kits; CXCR2 inhibitor SB250002; and mouse chemokine array kits were purchased from R&D Systems. Goat anti-mCXCR2 antiserum was kindly provided by Dr. Robert M. Strieter (School of Medicine, University of Virginia, Charlottesville, VA). Monoclonal anti–β-actin and anti–factor VIII–related Ag Abs, 3,3′,5,5′-tetramethylbenzidine, ExtrAvidin-peroxidase, DNAse, and collagenase were purchased from Sigma Life Sciences. Microtiter plates and Bouin's fixative were purchased from VWR International. Gelatin-precast Ready Gel Zymogram Gels were obtained from Bio-Rad Laboratories. Novex Zymogram Developing Buffer was obtained from Invitrogen (Life Technologies). Monoclonal anti–phospho–NF-κB–p65 (Ser^{536}) and polyclonal anti–p65-NF-κB Abs were purchased from Cell Signaling Technology. All the other reagents were obtained from commercial sources.

Animals

All experiments were approved by and conformed to the guidelines of the Animal Care and Use Committee of North Carolina Central University (Durham, NC). GRK6$^{-/-}$ and βarr2$^{-/-}$ mice (C57BL/6 background) were kindly provided by Dr. Robert J. Lefkowitz (Duke University Medical Center, Durham, NC). Male and female mice were evaluated, and control mice were age- and sex-matched littermates. All mice were genotyped at 21 d old; DNA samples were prepared from the tail tips with Extract-N-Amp tissue PCR kit from Sigma and subjected to triplex PCR as described previously (21, 22). The GRK6$^{-/-}$/βarr2$^{-/-}$ double-knockout mouse model was generated by backcrossing GRK6$^{-/-}$ and βarr2$^{-/-}$ animals. Double-knockout animals were confirmed by RT-PCR.

Heterotopic Lewis lung carcinoma model

LLC was a spontaneously occurring lung cancer in C57BL/6 mice. The CRL-1642 was routinely maintained in DMEM supplemented with 10% heat-inactivated FBS, 1.5 g/l sodium bicarbonate, 4 mM/l glutamine, 100 μg/ml streptomycin, and 100 IU/ml penicillin. GRK6$^{+/+}$ and GRK6$^{-/-}$ mice (6–8 wk, n = 14) were injected s.c. with LLC cells (5×10^5 cells in 100 μl). After each week, mice were euthanized by CO_2 asphyxiation; tumors were dissected from mice and measured with a Thorpe caliper (VWR). Tumor volume was calculated using the formula: Volume = $(d_1 \times d_2 \times d_3) \times 0.5236$, where d_n represents the three orthogonal diameter measurements (21, 23). Tumor and tissue specimens were either fixed in buffered formalin or processed for ELISA or FACS analysis.

Tail vein metastasis model

The LLC cells (3×10^5 viable cells per 100 μl) were injected via the tail vein of GRK6$^{+/+}$ and GRK6$^{-/-}$ mice (6–8 wk, n = 8). The mice were observed daily for any sign of respiratory distress and were euthanized by CO_2 after 4 wk. The lungs were removed and inflated with Bouin's fixative. The number of metastatic nodules on the lungs was counted with the aid of a dissecting microscope (21, 24). For survival experiments, GRK6$^{+/+}$ and GRK6$^{-/-}$ mice (6–8 wk, n = 14) were injected as described earlier and observed daily for mortality. The experiment was terminated when all the mice died of either group.

FACS analysis of single-cell isolates from heterotopic LLC tumors

Tumors were isolated from mice (n = 6), minced with scissors to fine slurry, and incubated in digestion buffer (RPMI 1640, 5% FBS, 1 mg/ml collagenase and 30 μg/ml DNAse) at 37°C for 45 min. Cells were washed, and cell counts and viability were determined using trypan blue exclusion on a hemocytometer. Cells (2×10^6) were resuspended in FACS analysis buffer and stained with PE-conjugated anti-mouse CD3, CD4, CD45, CD8a, NK1.1, Ly6, or factor VIII–related Ag Abs. Cells were also stained with rat anti-mouse CXCR2 and goat anti-rat PE-conjugated secondary Abs (21, 23). Stained cells were analyzed on a FACScan Flow Cytometer using Cell Quest software (BD Biosciences).

CXCL1/KC, CXCL2/MIP-2, CXCL12/SDF-1, VEGF, and MMP levels in tumors

Heterotopic LLC tumors (n = 10) were harvested 4 wk postinoculation. One gram of dissected tumors was homogenized in 10 ml PBS. The quantity of murine CXCL1/KC, CXCL2/MIP-2, CXCL12/SDF-1, VEGF, MMP-2, and MMP-9 present in tissue homogenates was determined by specific ELISA, using a modification of the double-ligand method, as previously described (21, 23). In brief, flat-bottom 96-well microtiter plates were coated with 100 μl/well of specific polyclonal anti-mouse CXCL1/KC, CXCL2/MIP-2, CXCL12/SDF-1, VEGF, MMP-2, and MMP-9 (1 μg/ml in coating buffer, pH 9.5) for 24 h at 4°C and then washed three times with PBS, pH 7.5, plus 0.05% Tween 20 (wash buffer). Plates were blocked with 1% BSA in PBS for 90 min at 37°C and then washed three times with wash buffer. A total of 100 μl supernatant from each homogenate was added in plates and then incubated at 37°C for 90 min. Plates were washed three times; 100 μl biotinylated polyclonal anti-murine CXCL1/KC, CXCL2/MIP-2, CXCL12/SDF-1, VEGF, MMP-2, and MMP-9 (diluted in PBS, pH 7.5, 0.05% Tween 20) was added and then incubated at 37°C for 45 min. Plates were washed three times; 100 μl ExtrAvidin-peroxidase conjugate was added and then incubated for another 45 min at 37°C. Plates were washed again, and 100 μl 3,3′,5,5′-tetramethylbenzidine chromogenic substrate was added. Plates were incubated at room temperature for 20–30 min, and the reactions were terminated by the addition of 100 μl/well of 1 M H_2SO_4. Plates were read at 450 nm in an automated microplate reader (Perkin Elmer). The amount of mouse CXCL1/KC, CXCL2/MIP-2, CXCL12/SDF-1, VEGF, MMP-2, and MMP-9 present was determined by interpolation of a standard curve generated by known amounts of recombinant mouse CXCL1/KC, CXCL2/MIP-2, CXCL12/SDF-1, VEGF, MMP-2, and MMP-9, respectively.

MMP-9 activity

MMP-9 activity was determined as previously reported (25, 26). In brief, tumor lysates (20 μg) or recombinant murine MMP-9 (5 ng), as positive control, were electrophoresed in 10% gelatin-precast Ready Gel Zymogram Gels (Bio-Rad Laboratories). The gels were washed twice in 2.5% Triton X-100 for 30 min and incubated overnight at 37°C in Novex Zymogram Developing Buffer (Life Technologies, Carlsbad, CA). The gels were stained with 0.1% Coomassie Blue (R250) for 1 h and then destained in 5% acetic acid, 10% methanol. The activity of the MMP-9 relative to the control standard was determined by densitometric scanning of the gels with a UV transilluminator (BioDoc-It Imaging System, UVP, Upland, CA), and the images were analyzed by Adobe Photoshop (Adobe Systems, Mountain View, CA).

Treatments in vivo

GRK6$^{+/+}$ and GRK6$^{-/-}$ mice (6–8 wk) were injected s.c. with LLC cells as outlined earlier. Mice (n = 6) were injected i.p. with 500 μl of either neutralizing goat anti-mouse CXCR2, control (preimmune) serum, or no treatment every day for 4 wk. In subsequent experiments, LLC tumor-bearing GRK6$^{+/+}$ and GRK6$^{-/-}$ mice (n = 5) were treated i.p. with the CXCR2 inhibitor SB225002 (5 mg/kg/day), control (PBS), or no treatment every day for 4 wk. Tumor volume was measured as described earlier.

Quantitation of microvessel density

Paraffin-embedded tumor tissues from GRK6$^{+/+}$ and GRK6$^{-/-}$ mice were processed for immunohistochemical localization of factor VIII–related Ag, as previously described (27). In brief, tissue sections were dewaxed with xylene and rehydrated through graded series of alcohol. Tissue sections were treated with 0.10 M citric acid buffer in a heated pressure cooker for 10 min. Slides were blocked with normal goat serum and overlaid with 1:500 dilution of either control (rabbit) or anti–factor VIII–related Ag Ab for overnight at 4°C. Slides were then rinsed and overlaid with secondary

biotinylated goat anti-rabbit IgG (1:200) and incubated for 60 min. After washing with PBS, slides were overlaid with a 1:200 dilution of ExtrAvidin-peroxidase conjugate and incubated for 60 min. 3′3-Diaminobenzedine tetrahydrochloride was used for chromogenic localization of factor VIII–related Ag. After optimal color development, sections were washed with sterile water, counterstained with Mayer's hematoxylin, and dehydrated into the graded series of alcohol and mounted. Quantitation of microvessel density was performed using the previously described method with slight modifications (27). Tumor specimens ($n = 10$) were scanned at low magnification (×20) to identify vascular hotspots. Areas of greatest vessel density (six from each specimen) were then examined under higher magnification (×200) and counted with the help of grid eyepiece. Any distinct areas of positive staining for factor VIII–related Ag were counted as single vessels. Results were expressed as the number of microvessels per square millimeter.

Immunoblotting

For GRK6 expression analysis, LLC cells, zymosan-elicited PMNs (1×10^6) isolated from GRK6$^{+/+}$ and GRK6$^{-/-}$ mice, WT RBL-2H, and GRK6-depleted RBL (RBL-GRK6$^{-/-}$), were lysed in radioimmune precipitation assay buffer and assayed for protein concentration. Twenty micrograms of proteins was resolved on 10% SDS-PAGE, transferred to nitrocellulose paper, probed with mouse monoclonal anti-GRK6 Ab, and detected with HRP-conjugated goat anti-mouse Ab and ECL. For NF-κB–p65 phosphorylation, zymosan-elicited PMNs (1×10^7) were treated with or without CXCL1/KC (1 μM) in PBS for 10 min at 37°C. Then cells were washed, lysed, and immunoblotted with either anti–phospho–NF-κB–p65 or anti–NF-κB–p65 (21).

Chemokine measurement in LLC cells

Chemokine levels were measured using the commercially available Mouse Chemokine Array (R&D Systems) according to the protocol supplied by the manufacturer. LLC cell lysates were prepared as described in the protocol and assayed for protein concentrations. Five hundred micrograms proteins were run on each array.

Statistical analyses

Results are expressed as mean ± SEM. Statistical analysis was performed using GraphPad Prism 5.0 (GraphPad Software, San Diego, CA). Differences between groups were determined using one-way ANOVA or Student t test (two-tailed), as appropriate. A p value <0.05 was considered statistically significant.

Results

GRK6 depletion enhanced tumorigenesis and metastasis

To assess the role of GRK6 in tumor development, we injected 6- to 8-wk-old male GRK6$^{-/-}$ mice and control littermates (GRK6$^{+/+}$) heterotopically with LLC cells (5×10^5) under the dorsal skin. Tumor size was measured 4 wk after injection. As shown in Fig. 1A, tumor growth occurred faster in GRK6$^{-/-}$ mice as compared with GRK6$^{+/+}$. Time course of tumor growth in both male (Fig. 1B) and female (Fig. 1C) mice showed a significant difference in tumor size relative to control animals. This result indicates that the actions of GRK6 oppose tumor growth in our s.c. tumor model.

We next determined the role of GRK6 deficiency in lung metastasis by measuring the number of metastatic nodules on the lungs. Colonization of the lung was significantly greater in GRK6$^{-/-}$ mice as compared with GRK6$^{+/+}$ (Fig. 2A). The number of metastatic tumor nodules was ~6-fold higher in lungs from GRK6$^{-/-}$ mice relative to WT animals (Fig. 2B). GRK6 deletion also caused a significant reduction in the median survival of GRK6$^{-/-}$ mice (~22 d) relative to the GRK6$^{+/+}$ mice (~40 d; Fig. 2C).

We also measured the expression of GRK6 in LLC tumor cells, peritoneal neutrophils isolated from GRK6$^{-/-}$ and GRK6$^{+/+}$ mice, control RBL-2H3 cells (RBL- GRK6$^{+/+}$), and RBL-2H3 cells in which GRK6 was stably knocked down by short hairpin RNA (RBL-GRK6$^{-/-}$) (19). As shown in Supplemental Fig. 1, GRK6 expression in LLC cells (*lane 3*) was similar to that of RBL-GRK6$^{+/+}$ cells (*lane 4*) and PMNs from GRK6$^{+/+}$ mice (*lane 1*). GRK6 expression was inhibited in PMNs from GRK6$^{-/-}$ (*lane 2*)

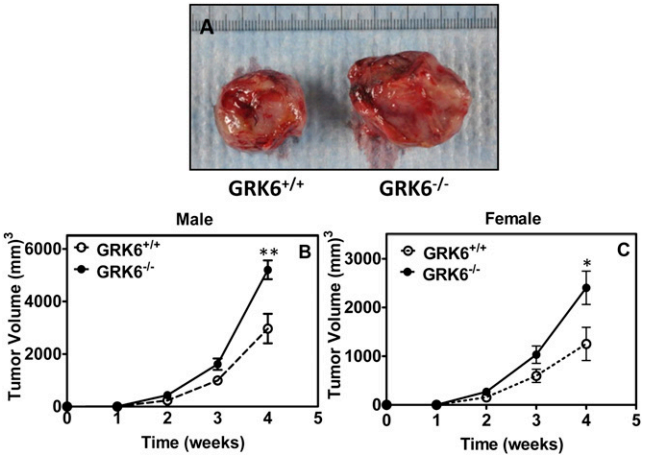

FIGURE 1. Knockdown of GRK6 promotes heterotopic LLC tumor growth. GRK6$^{+/+}$ and GRK6$^{-/-}$ mice ($n = 11$) were injected s.c. with LLC cells (1×10^5). Heterotopic tumor growth was measured weekly with a Thorpe caliper. Tumor volume was calculated using the formula: Volume = $(d_1 \times d_2 \times d_3) \times 0.5236$, where the d_n represents the three orthogonal diameter measurements. Representative photographs of tumor dissected from GRK6$^{+/+}$ and GRK6$^{-/-}$ mice (**A**). Heterotopic LLC tumor growth over 4 wk in male (centimeter scale) (**B**) and female (**C**) mice. The experiments were repeated three times with similar results. $*p < 0.05$, $**p < 0.005$.

mice, as well as RBL-GRK6$^{-/-}$ cells (*lane 5*). This result suggests that the effect of GRK6 inhibition in tumor growth is due to the host.

Effect of GRK6 depletion on chemokine, VEGF, and MMP expression

To determine the effect of GRK6 depletion on chemokine and proangiogenic factor expression, we measured the levels of CXCL1/KC, CXCL2/MIP-2, CXCL12/SDF-1, VEGF, MMP-2,

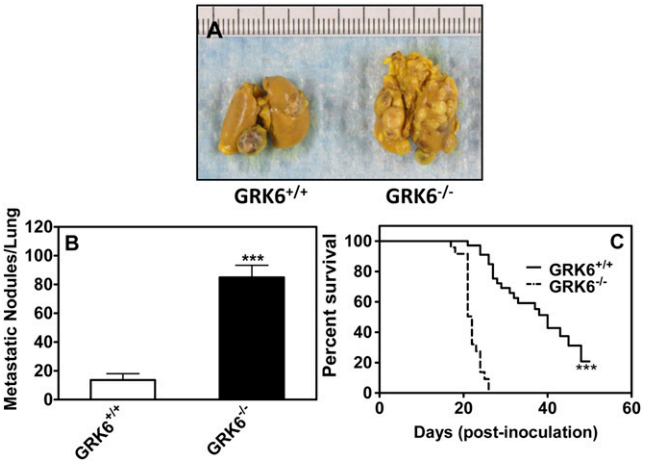

FIGURE 2. GRK6 inhibition increases lung metastasis and mortality. For lung metastasis (**A**), LLC cells (3×10^5) were injected via the tail vein of GRK6$^{+/+}$ and GRK6$^{-/-}$ mice ($n = 10$). The mice were euthanized by CO_2 after 4 wk; lungs were removed and inflated with Bouin's fixative. Photographs are representative of LLC cell colonization and growth in lungs of GRK6$^{+/+}$ and GRK6$^{-/-}$ mice (centimeter scale). (**B**) The number of metastatic nodules on the lungs was counted with the aid of a dissecting microscope. (**C**) For survival rate, mice ($n = 14$) were injected LLC cells via tail vein for lung metastasis as described earlier and observed daily up to 60 d for the mortality. GRK6$^{-/-}$ mice displayed decreased survival rate compared with GRK6$^{+/+}$. The experiments were repeated twice with similar results. $***p < 0.0001$.

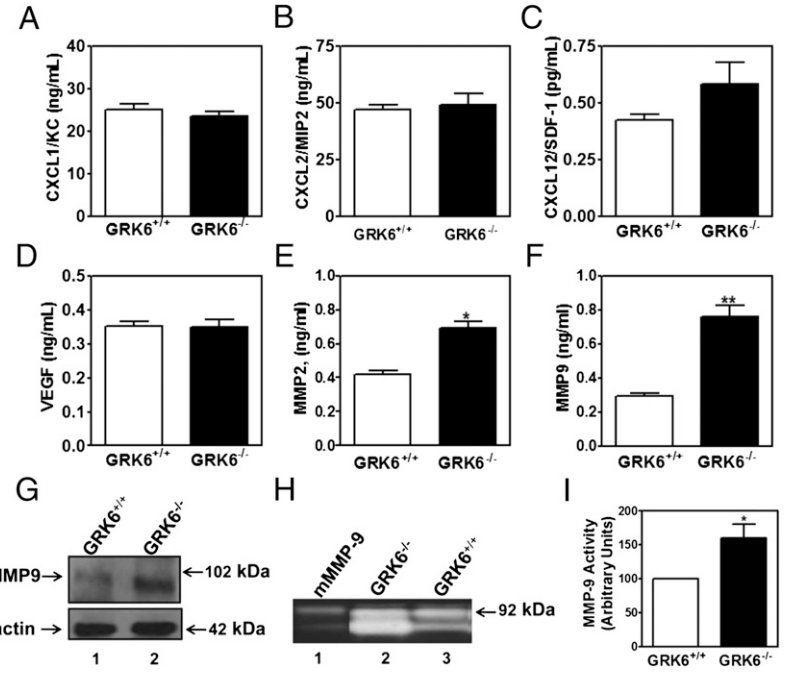

FIGURE 3. Effect of GRK6 deficiency on production of proangiogenic factors. Levels of CXCL1/KC (A), CXCL2/MIP-2 (**B**), CXCL12/SDF-1 (**C**), VEGF (**D**), MMP-2 (**E**), and MMP-9 (**F**) in the homogenate of heterotopic LLC tumors from GRK6$^{+/+}$ and GRK6$^{-/-}$ mice (n = 6) were determined by specific double Ab sandwich ELISA as described in *Materials and Methods*. (**G**) Tumor lysates were assayed for MMP-9 expression by immunoblotting. Twenty micrograms of proteins was resolved on 10% SDS-PAGE, transferred to nitrocellulose paper, and probed with rabbit polyclonal anti–MMP-9 Ab. The experiment was repeated twice with similar results. (**H**) Representative zymogram of MMP-2 and MMP-9 activity. Murine recombinant MMP-2 and MMP-9 (5 ng each, *lane 1*) or tumor lysates (20 μg) from GRK6$^{-/-}$ animals (*lane 2*) or WT GRK6$^{+/+}$ were subjected to electrophoresis without heat denaturation or thiol-reduction in 10% gelatin-precast Ready Gel Zymogram Gels and assayed for MMP activity as described in *Materials and Methods*. (**I**) MMP activity was calculated from MMP-9 and MMP-2 clear band density. Data shown are average from three independent experiments. *$p < 0.05$, **$p < 0.005$.

and MMP-9 in the homogenate of the LLC tumors from GRK6$^{-/-}$ and control littermates. No significant changes in the levels of expression of CXCL1/KC (Fig. 3A), CXCL2/MIP-2 (Fig. 3B), CXCL12/SDF-1 (Fig. 3C), or VEGF (Fig. 3D) were observed. MMP-2 (Fig. 3E) and MMP-9 (Fig. 3F) expression levels, however, were significantly enhanced in tumors from GRK6$^{-/-}$ animals relative to GRK6$^{+/+}$. The increased MMP-9 expression in GRK6$^{+/+}$ was further assessed by immunoblotting. As shown in Fig. 3G, tumor homogenate from GRK6$^{-/-}$ mice (*lane 2*) showed a marked increase in MMP-9 expression as compared with GRK6$^{+/+}$ (*lane 1*). MMP-9 activity in tumor homogenates was also examined using gelatin zymography. GRK6$^{-/-}$ mice (Fig. 3H, *lane 2*; Fig. 3I, closed bar) exhibited significantly greater MMP-9 activity relative to GRK6$^{+/+}$ (Fig. 3H, *lane 3*; Fig. 3I, open bar). Recombinant murine MMP-9 (Fig. 3H, *lane 1*) was used as positive control.

To further assess the role of GRK6 depletion in angiogenesis, we stained tumors with an Ab specific for factor VIII–related Ag for determination of microvessels density. Tumors from GRK6$^{-/-}$ mice (Fig. 4B, 4C, closed bar) showed a statistically significant increase in the number of microvessels density as compared with tumors from GRK6$^{+/+}$ mice (Fig. 4A, 4C, open bar).

Effect of GRK6 depletion on intratumor leukocyte infiltrations

We next analyze the intratumor leukocyte infiltration of cell isolates from LLC tumors of GRK6$^{-/-}$ and GRK6$^{+/+}$ mice. As shown in Table I, no significant difference was found in tumor infiltrating NK$^+$, CD3$^+$, CD4$^+$, CD45$^+$, and CD8a$^+$ in GRK6$^{-/-}$ as compared with GRK6$^{+/+}$ mice. However, significant increases were observed in PMN, CXCR2, and factor VIII–related Ag-expressing cells in GRK6$^{-/-}$ relative to GRK6$^{+/+}$ mice (Table I).

Inhibition of CXCR2 diminished the effect of GRK6 depletion in LLC tumor development

To assess the role of CXCR2 in GRK6-mediated tumor progression, we used a CXCR2 inhibitor SB225002 and a CXCR2-neutralizing Ab to block the receptor in the heterotopic model. GRK6$^{-/-}$ mice treated with SB225002 showed a significant decrease (~45%) in tumor size relative to nontreated animals (Fig. 5A, closed bars). Treatment of GRK6$^{+/+}$ animals with SB225002, however, had no significant effect in tumor size (Fig. 5A, open bars). Treatment of both GRK6$^{+/+}$ (Fig. 5B, open bars) and GRK6$^{-/-}$ (Fig. 5B, closed bars) mice with the anti-mouse CXCR2 Ab caused a significant decrease (~85% for GRK6$^{+/+}$ and ~73% for GRK6$^{-/-}$) in tumor size relative to untreated animals. The inhibitory effect of the murine CXCR2 Ab in tumor growth was greater than that of the pharmacological inhibitor SB225002 (~85 versus 45%), relative to WT animals. This is likely due to the dose of SB225002 used in these experiments (5 mg/kg/d). Greater inhibitory effects in tumor volume were obtained with higher doses, 7.5 and 10 mg/kg/d (data not shown). However, because of the reduced survival rates (80–100% of the

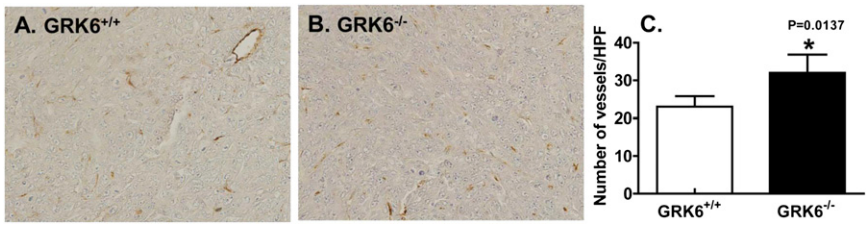

FIGURE 4. GRK6 deficiency promotes angiogenesis in LLC tumors. Heterotopic LLC tumors were dissected from GRK6$^{+/+}$ and GRK6$^{-/-}$ mice (n = 6) after 4 wk, fixed in 10% neutral-buffered formaldehyde, and embedded in paraffin. Tissue sections were immunostained with factor VIII–related Ag (**A**) GRK6$^{+/+}$ and (**B**) GRK6$^{-/-}$. Areas of greatest vessel density were examined under higher magnification (×200) and number of microvessels in 1.0-mm^2 area was counted by light microscope with a grid eyepiece (**C**). *$p < 0.05$.

Table I. FACS analysis of intratumor-infiltrating leukocyte subpopulations

	NK$^+$	CD3$^+$	CD4$^+$	CD45$^+$	CD8$^+$	PMN$^+$	CXCR2$^+$	Factor VIII
GRK6$^{+/+}$	2.71 ± 0.30	3.22 ± 0.569	3.53 ± 0.56	18.81 ± 1.30	1.68 ± 0.341	1.91 ± 0.42	17.92 ± 1.39	21.87 ± 2.29
GRK6$^{-/-}$	2.92 ± 0.29	4.01 ± 0.52	3.73 ± 0.69	26.78 ± 3.36	1.787 ± 0.50	4.88 ± 0.24**	30.09 ± 6.15*	37.44 ± 3.35**

Single-cell isolates from heterotopic LLC tumors from GRK6$^{+/+}$ and GRK$^{-/-}$ mice (n = 6) were stained for different leukocyte subpopulations (NK, CD3, CD4, CD45, CD8a, PMN, CXCR2, and factor VIII) and analyzed by FACScan Flow Cytometer using Cell Quest software.
*$p < 0.05$, **$p < 0.005$.

mice died between weeks 2 and 3) and the animals' aggressive behavior, we were limited to 5 mg/kg/d.

Are the effects of GRK6 and βarr2 inhibition in LLC growth additive?

We have previously shown that deletion of βarr2 promoted CXCR2-mediated angiogenesis, tumor progression, and metastasis (19). To determine whether the effects of βarr2 and GRK6 deficiency are additive, we generated a double-knockout (GRK6$^{-/-}$/βarr2$^{-/-}$) animal model (Fig. 6A). Six- to 8-wk-old male GRK6$^{-/-}$/βarr2$^{-/-}$, βarr2$^{-/-}$, and WT mice were injected heterotopically with LLC cells (5×10^5) under the dorsal skin, and tumor size was measured 3 wk after injection. As shown in Fig. 6B and 6C, GRK6$^{-/-}$/βarr2$^{-/-}$ mice exhibited faster tumor growth relative to βarr2$^{-/-}$ or WT animals.

We also examined the effect of CXCR2-neutralizing Ab in GRK6$^{-/-}$/βarr2$^{-/-}$ tumor growth. GRK6$^{-/-}$/βarr2$^{-/-}$ mice were injected heterotopically with LLC cells (2.5×10^5; the number of cells was reduced in half because of tumor size and concern by the animal facility) and treated daily with murine CXCR2 antiserum or goat serum (control). As shown in Fig. 7, mCXCR2-treated animals exhibited a significant decrease (~8%) in tumor growth as compared with control animals. This suggests that the effects of βarr2 and GRK6 deletion in CXCR2-mediated LLC tumor growth are additive.

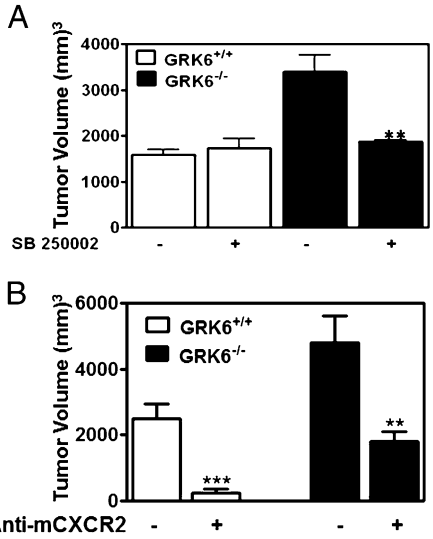

FIGURE 5. Blockade of CXCR2 inhibits heterotopic LLC tumor growth in mice. GRK6$^{+/+}$ and GRK6$^{-/-}$ mice were injected s.c. with LLC cells (1×10^5). For CXCR2 inhibition, mice were treated with (**A**) SB225002 or vehicle (n = 10) and (**B**) neutralizing anti-mCXCR2 serum (n = 6) or goat preimmune serum (n = 6) daily. After 4 wk, mice were euthanized by CO_2 and tumor volume was measured with a Thorpe caliper. **$p < 0.05$, ***$p < 0.001$.

Discussion

CXCR2 binds the proangiogenic ELR$^+$ chemokines to mediate cellular responses including chemotaxis and angiogenesis. Elevated expression levels of CXCR2 were observed in several cancer cell types including melanoma, lung, gastric, and colon carcinoma cells, and were shown to be associated with enhanced angiogenesis (28–32). Knockdown of CXCR2 in animal models of cancer was also shown to inhibit tumor growth and metastasis in several mouse models of cancers including melanoma, renal cell carcinoma, and LLC (23, 33, 34). We have previously shown that deletion of βarr2, a key regulator of CXCR2 functions, decreased receptor desensitization but promoted LLC progression and metastasis in mice (21). Our recent studies using GRK6-deficient RBL-2H3 cells and mouse models of inflammation have shown that GRK6-mediated phosphorylation of CXCR2 plays an important role in receptor desensitization and downregulation, as well as receptor-induced angiogenesis and wound closure (19). In this study, we investigated the role of GRK6 depletion in CXCR2-mediated tumorigenesis. The results in this article clearly demonstrated that, as was the case for βarr2$^{-/-}$ mice, deletion of GRK6 promoted CXCR2-mediated tumor progression and metastasis. First, heterotopically implanted LLC tumors in GRK6$^{-/-}$ mice showed a significant increase in tumor growth compared with WT mice (Fig. 1A–C). Second, in the tail vein metastasis assay, the number of metastatic nodules significantly increased in the lung of GRK6$^{-/-}$ mice (Fig. 2A, 2B). Third, survival rate of GRK6$^{-/-}$ mice decreased very significantly relative to GRK6$^{+/+}$ (Fig. 2C). Fourth, tumors from GRK6$^{-/-}$ mice showed significantly greater microvessels density as compared with WT animals (Fig. 4). And fifth, treatment of the mice with anti-CXCR2 Ab or the CXCR2-specific inhibitor, SB225002, abolished the effect of GRK6 depletion (Fig. 5).

Upregulation of ELR$^+$ chemokines in the tumor microenvironment is known to promote tumor angiogenesis (35, 36). In βarr2$^{-/-}$ animals, the increased tumor development and metastasis correlated with enhanced production of CXCL1/KC, CXCL2/MIP-2, and VEGF (21). Surprisingly, tumors from GRK6$^{-/-}$ animals displayed levels of CXCL1/KC, CXCL2/MIP-2, and VEGF similar to those of WT GRK6$^{+/+}$ mice (Fig. 3A–D). These results contrast with the βarr2$^{-/-}$ LLC model and suggest that the increased tumor growth and metastasis caused by GRK6 inhibition likely occurs via a mechanism different from that of induction of proangiogenic chemokine production. Indeed, although βarr2$^{-/-}$ mice displayed significant increase in NF-κB activity relative to βarr2$^{+/+}$ (21), CXCL1/KC-induced NF-κB p65 phosphorylation in peritoneal neutrophils from GRK6$^{-/-}$ animals was similar to that of control GRK6$^{+/+}$ (data not shown). Interestingly, both MMP-2 and MMP-9 were upregulated in GRK6$^{-/-}$ tumors relative to WT GRK6$^{+/+}$ (Fig. 3E–G). Several studies have shown that degradation of the extracellular matrix by MMPs is critical for endothelial cell angiogenesis (37–39). The CXCL8/CXCR2 axis was also shown to mediate tumor angiogenesis and metastasis via upregulation of MMP-2 and MMP-9 (40, 41). Peritoneal neutrophils and RBL-2H3 cells deficient in GRK6

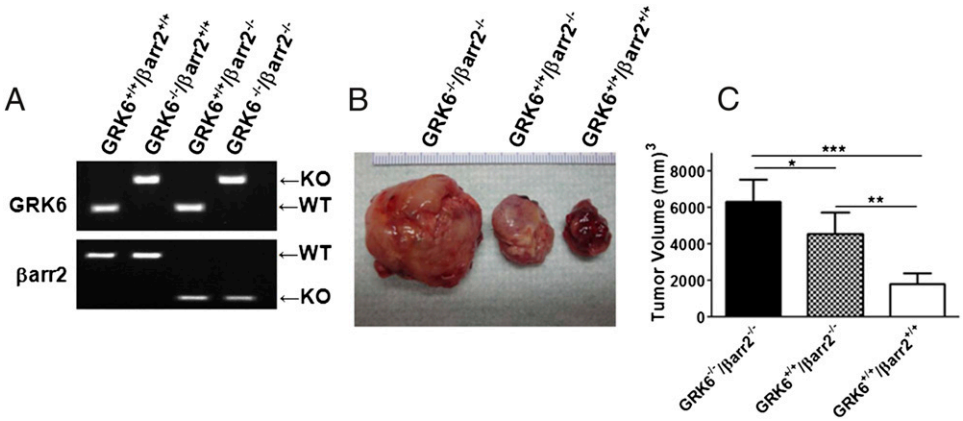

FIGURE 6. Effects of GRK6 and βarr2 knockdown in heterotopic LLC tumor growth. (**A**) Double-knockout GRK6$^{-/-}$/βarr2$^{-/-}$ mice were generated by backcrossing GRK6$^{-/-}$ with βarr2$^{-/-}$ animals and were genotyped by PCR analysis. (**B**) GRK6$^{-/-}$/βarr2$^{-/-}$, GRK6$^{+/+}$/βarr2$^{-/-}$, and WT (GRK6$^{+/+}$/βarr2$^{+/+}$) mice (n = 6–9) were injected s.c. with LLC cells (1×10^5). Heterotopic LLC tumors were grown over 4 wk and dissected. Shown are representative photographs of three experiments (centimeter scale). (**C**) After 4 wk, mice were euthanized by CO_2 and tumor volume was measured with a Thorpe caliper. $*p < 0.05$, $**p < 0.005$, $***p < 0.0001$.

exhibited increased CXCR2-mediated G protein activation and exocytosis (19). Therefore, it is possible that the increase in tumor angiogenesis and metastasis observed in GRK6-deficient animals is due to increased production of MMPs mediated by the host CXCR2 (Fig. 3E–G). Supporting that contention is that Western blot analysis and gelatin zymography showed significant increase in MMP-9 expression and activity in tumor homogenate from GRK6$^{-/-}$ mice relative to GRK6$^{+/+}$ animals (Fig. 3G–I).

The infiltration of immune cells into the tumor microenvironment is a key component of the tumor immunity (42). GRK6$^{-/-}$ depletion had no effect on T cell infiltration into the tumors but caused a significant increase in the level of PMNs (Table I). These observations also contrast with the βarr2$^{-/-}$ model of LLC, which displayed a significant decrease in T cell infiltration but no effect in PMN levels in the tumor microenvironment, relative to tumors from βarr2$^{+/+}$ mice (21). The role of PMNs in tumor infiltrates remains unclear. They have been associated with both better prognosis because of their phagocytic activities and poorer outcomes because of their abilities to release proangiogenic factors such as chemokines, VEGF, and MMPs (43, 44). Interestingly, the increased levels of PMNs observed in GRK6$^{-/-}$ tumor infiltrates in this study correlated with enhanced expression of MMP-2 and MMP-9 (Fig. 3E, 3F). Thus, the increased tumor growth and decreased survival rate of GRK6$^{-/-}$ animals compared with control GRK6$^{+/+}$ could be a consequence of PMNs increased activity resulting in greater secretion of proteases and tissue digestion, thereby promoting angiogenesis.

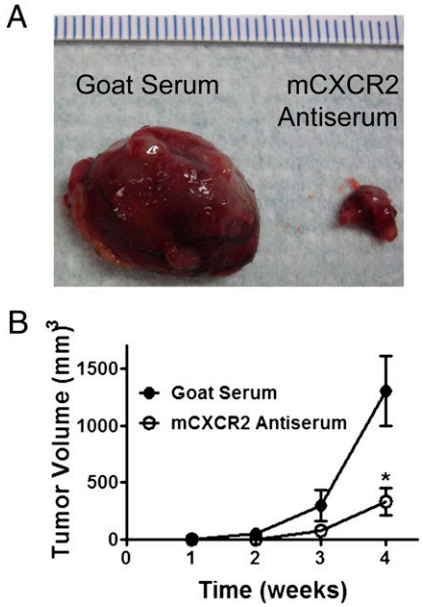

FIGURE 7. Anti-mCXCR2 inhibits tumor growth in GRK6$^{-/-}$/βarr2$^{-/-}$ animals. Male double-knockout GRK6$^{-/-}$/βarr2$^{-/-}$ mice were injected s.c. with LLC cells (0.5×10^5). For CXCR2 inhibition, mice were treated with neutralizing anti-mCXCR2 serum (n = 5) or goat preimmune serum (n = 5) daily. (**A**) Representative photographs of tumor dissected after 4 wk (centimeter scale). (**B**) Heterotopic LLC tumor growth was measured weekly with a Thorpe caliper. The experiments were repeated twice with similar results. $*p < 0.05$.

LLC cells express both GRK6 and CXCR2 (Supplemental Fig. 1) (23). Mice deficient in CXCR2 showed decreased tumor progression and metastasis (23). Thus, as was the case for the βarr2 knockout model, the enhanced tumor growth and metastasis exhibited by GRK6$^{-/-}$ animals is likely due to increased CXCR2 activity of the host endothelial cells. Supporting that contention is that immunostaining of tumor sections with anti–factor VIII–related Ag (specific for endothelial cells) showed a significant increase in microvessel density in GRK6$^{-/-}$ mice relative to GRK6$^{+/+}$ mice (Fig. 4). Keane et al. (23) have also shown that in LLC tumors, the cells expressing CXCR2 are predominantly the vascular endothelial cells.

Chemokine profiling of LLC cells using a mouse chemokine array revealed that these cells predominantly express CXCL1/KC (Supplemental Fig. 2). Whether LLC produced chemokines that play a role in the enhanced PMN infiltrations and/or increased tumor growth in GRK6$^{-/-}$ animals remains unclear. However, both GRK6$^{-/-}$ and GRK6$^{+/+}$ tumors showed similar levels of CXCL1/KC and CXCL2/MIP-2 expression (Fig. 3A, 3B). Furthermore, mice deficient in CXCR2 or treated with a CXCR2 blocking Ab displayed decreased chemokine expression and tumor growth, but similar levels of PMN in the tumor infiltrates (23). Raghuwanshi et al. (21) have also shown that tumors from βarr2$^{-/-}$ animals displayed increased CXCL1/KC and CXCL2/MIP-2, but similar level of PMNs in the tumor infiltrates. Taken together, these results further suggest that the effect of GRK6 deletion in tumor growth is due to increased CXCR2 activity in the host, but not the LLC cells.

Because the effects of GRK6 and βarr2 in CXCR2-induced tumor growth appeared to be mediated via distinct mechanisms, we hypothesized that deletion of the two molecules could have an additive effect. Indeed, the double-knockout GRK6$^{-/-}$βarr2$^{-/-}$ displayed tumor growth at a faster rate than those of the single-knockout animals (Fig. 6). The size of the GRK6$^{-/-}$βarr2$^{-/-}$ tumors at week 3 was similar to those of βarr2$^{-/-}$ or GRK6$^{-/-}$ at week 4 (data not shown). These results further indicate that CXCR2 modulate LLC tumor development through different mechanisms. One could be through βarr2-mediated regulation of NF-κB and expression of proangiogenic factors (21), and another through activation of GRK6 and production of MMPs.

In summary, the data in this article demonstrate that GRK6 plays a feedback regulatory role in CXCR2-mediated tumor development, invasion, and metastasis. In contrast with βarr2, these processes appear to be mediated through increased activity of CXCR2 resulting in greater production of matrix MMPs and enhanced angiogenesis. Both CXCR1 and CXCR2 were shown to mediate angiogenesis via increased MMP production (40, 41). Thus, an unanswered question is whether GRK6 deletion would also enhance CXCR1-mediated tumor growth? To date, conflicting reports exist concerning the expression and function of a murine homolog of CXCR1 (45–47). Fan et al. (47) have recently identified a possible mouse CXCR1 that binds CXCL6/GCP-2 and CXCL8/IL-8 with high affinity. Studies in RBL-2H3 cell stably expressing CXCR1, however, have shown that the receptor couples predominantly to GRK2 to mediate and regulate cellular responses (19). Therefore, it is unlikely that deletion of GRK6 would have a significant effect in CXCR1-mediated tumor growth and metastasis.

Acknowledgments

We thank Dr. Robert J. Lefkowitz (Howard Hughes Medical Institute, Duke University Medical Center, Durham, NC) for providing the GRK6 and βarr2-deficient mouse models, Dr. Robert M. Strieter (School of Medicine, University of Virginia, Charlottesville, VA) for anti-mouse CXCR2 antisera, and Dr. Ann Richmond (Vanderbilt University) for critical reading of the manuscript. We are very thankful to Kimberly M. Malloy (JLC Biomedical/Biotechnology Research Institute, North Carolina Central University, Durham, NC) for technical support.

Disclosures

The authors have no financial conflicts of interest.

References

1. Vroon, A., C. J. Heijnen, and A. Kavelaars. 2006. GRKs and arrestins: regulators of migration and inflammation. *J. Leukoc. Biol.* 80: 1214–1221.
2. Reiter, E., and R. J. Lefkowitz. 2006. GRKs and beta-arrestins: roles in receptor silencing, trafficking and signaling. *Trends Endocrinol. Metab.* 17: 159–165.
3. Pitcher, J. A., N. J. Freedman, and R. J. Lefkowitz. 1998. G protein-coupled receptor kinases. *Annu. Rev. Biochem.* 67: 653–692.
4. Koch, W. J., J. Inglese, W. C. Stone, and R. J. Lefkowitz. 1993. The binding site for the beta gamma subunits of heterotrimeric G proteins on the beta-adrenergic receptor kinase. *J. Biol. Chem.* 268: 8256–8260.
5. Luttrell, L. M., B. E. Hawes, K. Touhara, T. van Biesen, W. J. Koch, and R. J. Lefkowitz. 1995. Effect of cellular expression of pleckstrin homology domains on Gi-coupled receptor signaling. *J. Biol. Chem.* 270: 12984–12989.
6. Eichmann, T., K. Lorenz, M. Hoffmann, J. Brockmann, C. Krasel, M. J. Lohse, and U. Quitterer. 2003. The amino-terminal domain of G-protein-coupled receptor kinase 2 is a regulatory Gbeta gamma binding site. *J. Biol. Chem.* 278: 8052–8057.
7. Premont, R. T., A. D. Macrae, R. H. Stoffel, N. Chung, J. A. Pitcher, C. Ambrose, J. Inglese, M. E. MacDonald, and R. J. Lefkowitz. 1996. Characterization of the G protein-coupled receptor kinase GRK4. Identification of four splice variants. *J. Biol. Chem.* 271: 6403–6410.
8. Premont, R. T., W. J. Koch, J. Inglese, and R. J. Lefkowitz. 1994. Identification, purification, and characterization of GRK5, a member of the family of G protein-coupled receptor kinases. *J. Biol. Chem.* 269: 6832–6841.
9. Stoffel, R. H., R. R. Randall, R. T. Premont, R. J. Lefkowitz, and J. Inglese. 1994. Palmitoylation of G protein-coupled receptor kinase, GRK6. Lipid modification diversity in the GRK family. *J. Biol. Chem.* 269: 27791–27794.
10. Baggiolini, M., B. Dewald, and B. Moser. 1997. Human chemokines: an update. *Annu. Rev. Immunol.* 15: 675–705.
11. Murphy, P. M., M. Baggiolini, I. F. Charo, C. A. Hébert, R. Horuk, K. Matsushima, L. H. Miller, J. J. Oppenheim, and C. A. Power. 2000. International union of pharmacology. XXII. Nomenclature for chemokine receptors. *Pharmacol. Rev.* 52: 145–176.
12. Strieter, R. M., P. J. Polverini, S. L. Kunkel, D. A. Arenberg, M. D. Burdick, J. Kasper, J. Dzuiba, J. Van Damme, A. Walz, D. Marriott, et al. 1995. The functional role of the ELR motif in CXC chemokine-mediated angiogenesis. *J. Biol. Chem.* 270: 27348–27357.
13. Strieter, R. M., M. D. Burdick, J. Mestas, B. Gomperts, M. P. Keane, and J. A. Belperio. 2006. Cancer CXC chemokine networks and tumour angiogenesis. *Eur. J. Cancer* 42: 768–778.
14. Richardson, R. M., B. C. Pridgen, B. Haribabu, H. Ali, and R. Snyderman. 1998. Differential cross-regulation of the human chemokine receptors CXCR1 and CXCR2. Evidence for time-dependent signal generation. *J. Biol. Chem.* 273: 23830–23836.
15. Richardson, R. M., R. J. Marjoram, L. S. Barak, and R. Snyderman. 2003. Role of the cytoplasmic tails of CXCR1 and CXCR2 in mediating leukocyte migration, activation, and regulation. *J. Immunol.* 170: 2904–2911.
16. Fan, G. H., W. Yang, X. J. Wang, Q. Qian, and A. Richmond. 2001. Identification of a motif in the carboxyl terminus of CXCR2 that is involved in adaptin 2 binding and receptor internalization. *Biochemistry* 40: 791–800.
17. Nasser, M. W., R. J. Marjoram, S. L. Brown, and R. M. Richardson. 2005. Cross-desensitization among CXCR1, CXCR2, and CCR5: role of protein kinase C-epsilon. *J. Immunol.* 174: 6927–6933.
18. Richardson, R. M., R. A. DuBose, H. Ali, E. D. Tomhave, B. Haribabu, and R. Snyderman. 1995. Regulation of human interleukin-8 receptor A: identification of a phosphorylation site involved in modulating receptor functions. *Biochemistry* 34: 14193–14201.
19. Raghuwanshi, S. K., Y. Su, V. Singh, K. Haynes, A. Richmond, and R. M. Richardson. 2012. The chemokine receptors CXCR1 and CXCR2 couple to distinct G protein-coupled receptor kinases to mediate and regulate leukocyte functions. *J. Immunol.* 189: 2824–2832.
20. Su, Y., S. K. Raghuwanshi, Y. Yu, L. B. Nanney, R. M. Richardson, and A. Richmond. 2005. Altered CXCR2 signaling in beta-arrestin-2-deficient mouse models. *J. Immunol.* 175: 5396–5402.
21. Raghuwanshi, S. K., M. W. Nasser, X. Chen, R. M. Strieter, and R. M. Richardson. 2008. Depletion of beta-arrestin-2 promotes tumor growth and angiogenesis in a murine model of lung cancer. *J. Immunol.* 180: 5699–5706.
22. Fong, A. M., R. T. Premont, R. M. Richardson, Y. R. Yu, R. J. Lefkowitz, and D. D. Patel. 2002. Defective lymphocyte chemotaxis in beta-arrestin2- and GRK6-deficient mice. *Proc. Natl. Acad. Sci. USA* 99: 7478–7483.
23. Keane, M. P., J. A. Belperio, Y. Y. Xue, M. D. Burdick, and R. M. Strieter. 2004. Depletion of CXCR2 inhibits tumor growth and angiogenesis in a murine model of lung cancer. *J. Immunol.* 172: 2853–2860.
24. Elkin, M., and I. Vlodavsky. 2001. Tail vein assay of cancer metastasis. *Curr. Protoc. Cell Biol.* Chapter 19:Unit 19.2.
25. Schmalfeldt, B., D. Prechtel, K. Härting, K. Späthe, S. Rutke, E. Konik, R. Fridman, U. Berger, M. Schmitt, W. Kuhn, and E. Lengyel. 2001. Increased expression of matrix metalloproteinases (MMP)-2, MMP-9, and the urokinase-type plasminogen activator is associated with progression from benign to advanced ovarian cancer. *Clin. Cancer Res.* 7: 2396–2404.
26. Murase, S., and R. D. McKay. 2012. Matrix metalloproteinase-9 regulates survival of neurons in newborn hippocampus. *J. Biol. Chem.* 287: 12184–12194.
27. Arenberg, D. A., S. L. Kunkel, P. J. Polverini, M. Glass, M. D. Burdick, and R. M. Strieter. 1996. Inhibition of interleukin-8 reduces tumorigenesis of human non-small cell lung cancer in SCID mice. *J. Clin. Invest.* 97: 2792–2802.
28. Varney, M. L., S. L. Johansson, and R. K. Singh. 2006. Distinct expression of CXCL8 and its receptors CXCR1 and CXCR2 and their association with vessel density and aggressiveness in malignant melanoma. *Am. J. Clin. Pathol.* 125: 209–216.
29. Varney, M. L., A. Li, B. J. Dave, C. D. Bucana, S. L. Johansson, and R. K. Singh. 2003. Expression of CXCR1 and CXCR2 receptors in malignant melanoma with different metastatic potential and their role in interleukin-8 (CXCL-8)-mediated modulation of metastatic phenotype. *Clin. Exp. Metastasis* 20: 723–731.
30. Eck, M., B. Schmausser, K. Scheller, S. Brändlein, and H. K. Müller-Hermelink. 2003. Pleiotropic effects of CXC chemokines in gastric carcinoma: differences in CXCL8 and CXCL1 expression between diffuse and intestinal types of gastric carcinoma. *Clin. Exp. Immunol.* 134: 508–515.
31. Zhu, Y. M., S. J. Webster, D. Flower, and P. J. Woll. 2004. Interleukin-8/CXCL8 is a growth factor for human lung cancer cells. *Br. J. Cancer* 91: 1970–1976.
32. Wislez, M., N. Fujimoto, J. G. Izzo, A. E. Hanna, D. D. Cody, R. R. Langley, H. Tang, M. D. Burdick, M. Sato, J. D. Minna, et al. 2006. High expression of ligands for chemokine receptor CXCR2 in alveolar epithelial neoplasia induced by oncogenic kras. *Cancer Res.* 66: 4198–4207.
33. Singh, S., M. Varney, and R. K. Singh. 2009. Host CXCR2-dependent regulation of melanoma growth, angiogenesis, and experimental lung metastasis. *Cancer Res.* 69: 411–415.
34. Mestas, J., M. D. Burdick, K. Reckamp, A. Pantuck, R. A. Figlin, and R. M. Strieter. 2005. The role of CXCR2/CXCR2 ligand biological axis in renal cell carcinoma. *J. Immunol.* 175: 5351–5357.
35. Addison, C. L., T. O. Daniel, M. D. Burdick, H. Liu, J. E. Ehlert, Y. Y. Xue, L. Buechi, A. Walz, A. Richmond, and R. M. Strieter. 2000. The CXC chemokine receptor 2, CXCR2, is the putative receptor for ELR+ CXC chemokine-induced angiogenic activity. *J. Immunol.* 165: 5269–5277.

36. Heidemann, J., H. Ogawa, M. B. Dwinell, P. Rafiee, C. Maaser, H. R. Gockel, M. F. Otterson, D. M. Ota, N. Lugering, W. Domschke, and D. G. Binion. 2003. Angiogenic effects of interleukin 8 (CXCL8) in human intestinal microvascular endothelial cells are mediated by CXCR2. *J. Biol. Chem.* 278: 8508–8515.
37. Sang, Q. X. A. 1998. Complex role of matrix metalloproteinases in angiogenesis. *Cell Res.* 8: 171–177.
38. Rundhaug, J. E. 2003. Matrix metalloproteinases, angiogenesis, and cancer: commentary re: A. C. Lockhart et al., Reduction of wound angiogenesis in patients treated with BMS-275291, a broad spectrum matrix metalloproteinase inhibitor. Clin. Cancer Res., 9: 00-00, 2003. *Clin. Cancer Res.* 9: 551–554.
39. Rundhaug, J. E. 2005. Matrix metalloproteinases and angiogenesis. *J. Cell. Mol. Med.* 9: 267–285.
40. Li, A., S. Dubey, M. L. Varney, B. J. Dave, and R. K. Singh. 2003. IL-8 directly enhanced endothelial cell survival, proliferation, and matrix metalloproteinases production and regulated angiogenesis. *J. Immunol.* 170: 3369–3376.
41. Li, A., M. L. Varney, J. Valasek, M. Godfrey, B. J. Dave, and R. K. Singh. 2005. Autocrine role of interleukin-8 in induction of endothelial cell proliferation, survival, migration and MMP-2 production and angiogenesis. *Angiogenesis* 8: 63–71.
42. Chiou, S. H., B. C. Sheu, W. C. Chang, S. C. Huang, and H. Hong-Nerng. 2005. Current concepts of tumor-infiltrating lymphocytes in human malignancies. *J. Reprod. Immunol.* 67: 35–50.
43. Scapini, P., J. A. Lapinet-Vera, S. Gasperini, F. Calzetti, F. Bazzoni, and M. A. Cassatella. 2000. The neutrophil as a cellular source of chemokines. *Immunol. Rev.* 177: 195–203.
44. Scapini, P., M. Morini, C. Tecchio, S. Minghelli, E. Di Carlo, E. Tanghetti, A. Albini, C. Lowell, G. Berton, D. M. Noonan, and M. A. Cassatella. 2004. CXCL1/macrophage inflammatory protein-2-induced angiogenesis in vivo is mediated by neutrophil-derived vascular endothelial growth factor-A. *J. Immunol.* 172: 5034–5040.
45. Fu, W., Y. Zhang, J. Zhang, and W.-F. Chen. 2005. Cloning and characterization of mouse homolog of the CXC chemokine receptor CXCR1. *Cytokine* 31: 9–17.
46. Moepps, B., E. Nuesseler, M. Braun, and P. Gierschik. 2006. A homolog of the human chemokine receptor CXCR1 is expressed in the mouse. *Mol. Immunol.* 43: 897–914.
47. Fan, X., A. C. Patera, A. Pong-Kennedy, G. Deno, W. Gonsiorek, D. J. Manfra, G. Vassileva, M. Zeng, C. Jackson, L. Sullivan, et al. 2007. Murine CXCR1 is a functional receptor for GCP-2/CXCL6 and interleukin-8/CXCL8. *J. Biol. Chem.* 282: 11658–11666.